Evolution of Ni : B 2 O 3 core-shell structure and magnetic properties on devitrification of amorphous NiB particles in air

Vidyadhar Singh and V. Srinivas

Articles you may be interested in

Synthesis and magnetic characterization of Co-NiO-Ni core-shell nanotube arrays
J. Appl. Phys. **110**, 073912 (2011); 10.1063/1.3646491

Structure and magnetic properties of chemically prepared mixtures of crystalline and amorphous Fe(B) nanoparticles
J. Appl. Phys. **97**, 10F501 (2005); 10.1063/1.1847151

Grain size dependence of magnetic properties in shock synthesized bulk Pr 2 Fe 14 B ∕ α - Fe nanocomposites
J. Appl. Phys. **96**, 3452 (2004); 10.1063/1.1782956

Mössbauer study of the magnetism and structure of amorphous and nanocrystalline Fe 81−x Ni x Zr 7 B 12 (x=10–40) alloys
J. Appl. Phys. **94**, 638 (2003); 10.1063/1.1578701

Effect of Co substitution on the crystallization behavior and magnetic properties of melt-spun (Pr,Tb) 2 (Fe,Nb,Zr) 14 B /α- Fe nanocomposites
J. Appl. Phys. **93**, 7978 (2003); 10.1063/1.1558273

Evolution of Ni:B$_2$O$_3$ core-shell structure and magnetic properties on devitrification of amorphous NiB particles in air

Vidyadhar Singh and V. Srinivas[a)]

Department of Physics and Meteorology, Indian Institute of Technology, Kharagpur 721302, India

The Ni:B$_2$O$_3$ nanoparticles have been synthesized by a novel two-step chemical reduction method, under ambient conditions and subsequent annealing in air. The evolution of this structure has been followed through a sequence of annealing treatments. Structural and magnetic investigations on as-prepared and annealed samples revealed that as-prepared samples are weakly magnetic and develop into spherical ferromagnetic entities with superior magnetic properties. The saturation magnetization ($M_s \sim 42$ emu/g) and coercivity ($H_c \sim 482$ Oe) at room temperature clearly suggest that the air annealed (500 °C) samples are protected from the oxidation due to formation of B$_2$O$_3$ protective layer. The magnetization results are consistent with the observed microstructural changes and satisfactorily explained on the basis of a core-shell model, where we consider each particle as a magnetically heterogeneous system consisting of a ferromagnetic core of Ni and nonmagnetic shell of B$_2$O$_3$. These results suggest that this kind of nanocomposite systems might have significant potential as a recording media. © *2009 American Institute of Physics*. [doi:10.1063/1.3212540]

I. INTRODUCTION

Synthesis and functionalization of nanoparticles (NPs) of various sizes and shapes has received considerable interest in recent years because of their potential applications in high density magnetic recording media, catalysts, ferrofluids, medical diagnostics, pigments in paints and ceramics, and solid fuels.[1–3] The frequently encountered obstacle during synthesis of metal NPs is the spontaneous production of oxides, forming what is known as a "core-shell" structure. NPs having core-shell morphology are of interest in their own right and have been the subject of extensive research in the recent past.[2,4] The presence of a dielectric shell around at least part of the metallic core severely delays the oxidation and appears to be the main reason for their good high temperature stability. In addition to this, when ferromagnetic (FM) particles are embedded in a metal, semiconducting, or insulator matrix, the matrix is expected to introduce an extra degree of freedom that can be used to tune the properties of the embedded particles or the composite as a whole. It is an irrefutable fact that a passivating oxide layer on FM NPs plays a crucial role in magnetic properties, while rough estimates show that every oxygen atom destroys the contribution of one Ni atom to ferromagnetism and leads to a strong decrease in magnetization. On the other hand, presence of magnetic-oxide capping layer on magnetic NPs leads to large exchange bias effects and helps in rising the superparamagnetic (SPM) blocking temperature.[2,5] Therefore, there have also been studies on transition metal–transition metal oxide systems [Co–CoO,[5] Fe–FeO (Ref. 6)] where it was shown that the magnetic, optical, and electrical transport characteristics can be tailored by changing the relative dimensions of the core and shell in the NPs. The metallic magnetic NPs embedded in a nonmagnetic insulator matrix, such as SiO$_2$,[7]

Al$_2$O$_3$,[8] C,[9] BN,[10] and B$_2$O$_3$ (Refs. 11–13) matrices are of significant importance for industrial applications. The nonmagnetic insulating shell inhibits the interparticle interactions allowing one to investigate true magnetic behavior of the isolated magnetic particles. Luo *et al.*[11] have synthesized nanocomposite Fe/Pt:B$_2$O$_3$ thin films consisting of Fe:Pt grains embedded in a glassy B$_2$O$_3$ matrix through magnetron sputter technique and subsequent heat treatment. Their studies on microstructure and magnetic properties of Fe/Pt:B$_2$O$_3$ thin films indicated that the magnetic properties of the films strongly depend on volume fraction of B$_2$O$_3$ present in the composite, which led them to conclude that this nanocomposite system has significant potential as a high density recording media.

Recently composition-partial oxygen pressure diagram of Ni–B–O system has been investigated and it was proposed that with suitable heat treatment, the Ni-rich binary Ni–B alloys could be converted into Ni+B$_2$O$_3$ composites.[14] On the other hand, the crystallization process of Ni-rich Ni–B amorphous alloys has also been extensively studied.[15] These studies suggest that during devitrification of *a*-Ni–B ribbon, Ni-rich nanocrystallites nucleate until most of the boron is segregated.[16] Among the various synthesis techniques,[13,17–20] chemical reduction method[16,17,19] is widely used for the production of amorphous and nanocrystalline particles with relatively narrow size distribution. The devitrification behavior of *a*-Ni–B powders produced through borohydride reduction method has been investigated and found to be similar to that of amorphous ribbons samples produced by rapid solidification technique.[15,20–24] From these studies two glass forming composition ranges have been established in Ni–B alloy system. The first is around 17 at. % of B and the second is between 30 and 40 at. % B. The division of two groups had also been identified through the magnetic studies, though the interpretation of magnetic properties of Ni–B composition around 18.5 at. % of B has remained controversial. Bakonyi

---

a)Electronic mail: veeturi@phy.iitkgp.ernet.in.

et al.[21] have suggested that at a critical concentration of 81.5 at. % of Ni in Ni–B alloy the onset of spontaneous magnetic order occurs and suggested that such a magnetic behavior arises due to the presence of Ni-rich SPM particles embedded in the paramagnetic (PM) matrix. Subsequently, Muniz and co-workers[22,24] not only confirmed the existence of the SPM particles but also suggested the increase in SPM component due to growing population of Ni-rich nuclei on annealing at temperatures below 400 °C. The development of these magnetic inhomogeneities influenced by the composition of the matrix and by the synthesis techniques adopted. Most of the investigations in the literature focused on the samples prepared by rapid solidification processes and few are on samples prepared through chemical reduction method. In fact devitrification of amorphous ribbons results in formation of a composite with superior properties. Since amorphous freestanding particles can be obtained from chemical synthesis methods, one can develop nanoalloys or core-shell structured particles from these freestanding isolated particles via suitable heat treatment. Thus, developing a new and simple synthesis route for the production of core-shell type particles and investigation of stability and magnetic properties is of great importance for the present day magnetic industry.

In this article we present a simple and versatile chemical method for producing freestanding amorphous particles of Ni–B by reducing a 0.1 M aqueous $NiCl_2$ solution by the borohydride reduction method. The "as-prepared" *a*-Ni–B particles composition is observed to be in the vicinity of glass forming range, along with nascent oxygen. We have investigated in some detail as to how the structure and magnetic properties evolve when the samples are subjected to thermal treatment in air. By annealing the as-prepared powders in air at a suitable temperature $Ni:B_2O_3$ core-shell structured spherical magnetic particles have been developed. To corroborate our structural data, we have also performed the magnetic measurements on as-prepared and air annealed samples. Finally, a phenomenological model has been proposed that explains consistently all results obtained in the present study.

II. EXPERIMENT PROCEDURE

Fine powders of Ni–B were synthesized by reduction in aqueous solutions of metallic salts of $NiCl_2$ (Alfa, 99%:0.1 M) with $NaBH_4$ (Alfa, 98%:1 M) solution controlling the molarity, Ni^{2+}/BH_4^- ratio and *p*H of the precursors. The reduction was performed in air atmosphere by adding the $NaBH_4$ solution drop-by-drop to the metal ion solution. An excess of $NaBH_4$ with respect to the stochiometric reduction quantity was used in order to obtain the total reduction in the transition metal ions. The solution was vigorously stirred and instantaneous exothermic reaction ensued with the formation of black slurries with evolution of H_2 gas. The average temperature of the solution rises by 10–20 °C above room temperature. However, the dropwise addition of $NaBH_4$ controls the reaction and maintains the average temperature of the solution in the vicinity of room temperature. The resulting black slurries were washed with distilled water to remove
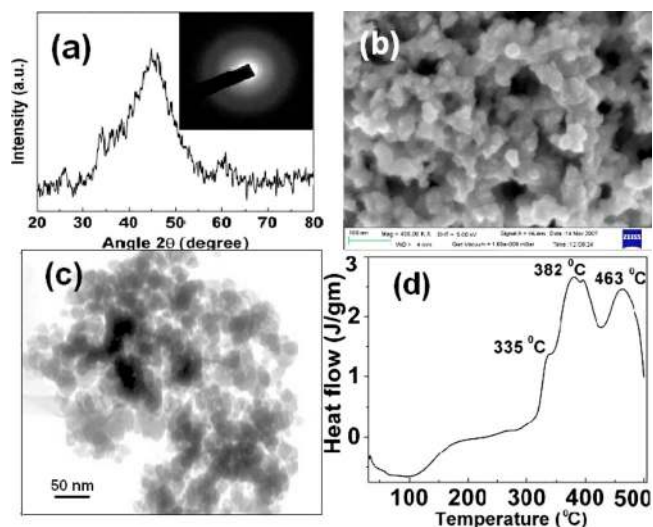

FIG. 1. (Color online) (a) X-ray diffractogram. Inset: SAED pattern showing amorphous nature. (b) FESEM surface topograph. (c) TEM micrograph. (d) DSC profile of as-prepared sample.

residual ions, and then rinsed with acetone to remove water and to restrain the surface oxidation. Finally sample was dried under vacuum 10–20 mbar at room temperature. After being dried for 48 h in air, the final product referred as-prepared sample in the following text. The as-prepared sample was annealed at 300, 400, and 500 °C for 1 h in vacuum as well as in air, to study the evolution of crystalline phases and phase transformations.

The structure of the sample is studied by x-ray diffraction (XRD) using Pan-analytical X'pert Pro XRD system (PW 3040), with filtered Cu $K\alpha_1$ radiation of wavelength λ =0.15406 nm. Thermal stability of the as-prepared sample has been investigated using differential scanning calorimeter (DSC) (Perkin Elmer Instruments) in the temperature range 30–500 °C by maintaining the heating rate 10 °C/min. The constituents of the as-prepared and annealed samples were analyzed by an electron probe x-ray microanalyzer (EPMA) (CAMECA–SX100) at 15 kV operating voltage. The particle size, morphology and chemical composition were evaluated by a transmission electron microscope (TEM) with an acceleration voltage of 200 kV (JEOL, JEM-2100) and energy-dispersive x-ray spectrometer. The size and surface topology was investigated with a field emission scanning electron microscope (FESEM) (Carl ZEISS-SUPRA 40) at 5 kV. The magnetization data as a function of applied fields up to 8 kOe and temperatures down to 20 K was recorded using a vibrating sample magnetometer (PARC made, model-155). Temperature variation in ac susceptibility data was taken by using homemade mutual inductance bridge and a close cycle helium cryostat (American Cryogenics, model 1768) in the temperature range 12–300 K.

III. RESULTS

A. Structural properties

Figure 1(a) depicts the x-ray diffractogram of as-prepared Ni–B fine particles. The diffractogram exhibits a broad halo in the vicinity of $2\theta \sim 45°$ suggest that the as-
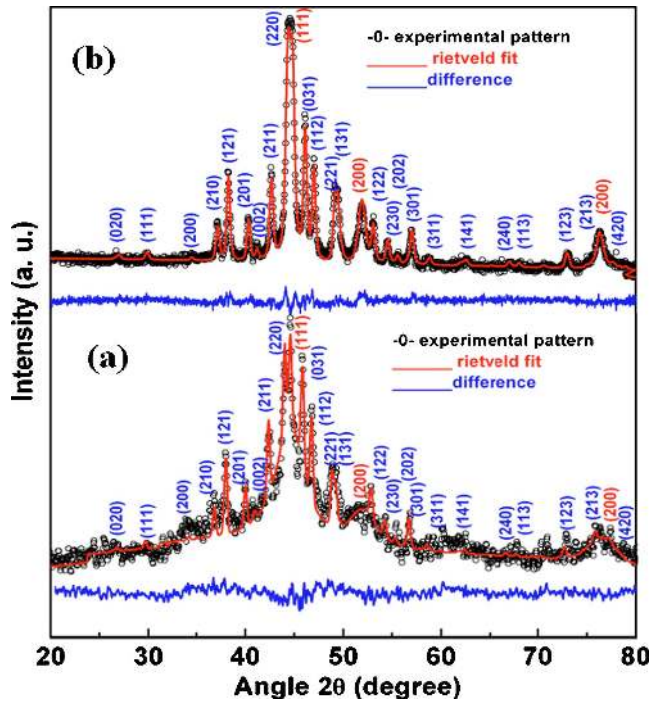
FIG. 2. (Color online) (a) X-ray diffractogram of sample at 350 °C (*in situ*). (b) Room temperature diffractogram of vacuum annealed at 400 °C for 1 h. Rietveld analysis of data (solid line) and obtained residues are shown plots.

TABLE I. Rietveld refinement parameters obtained from the fits to the data in Fig. 2.

Sample	350 °C		400 °C	
Phase	Ni$_3$B	Ni	Ni$_3$B	Ni
Space group	*Pnma*(62)	*Fm-3m*(125)	*Pnma*(62)	*Fm-3m*(125)
Lattice constant (Å)	a=5.22(1)	a=3.53(1)	a=5.213(1)	a=3.5260(5)
	b=6.63(1)		b=6.620(1)	
	c=4.39(8)		c=4.394(1)	
Crystallite size (nm)	19	9	25	12
Weight percentage	79	21	68	32
V/10^6 pm^3	152	43.9	151.58	43.84
R (profile)/%	8.88952		2.0876	
R (weighted profile)/%	11.06824		2.6326	

prepared sample is Ni-rich, while the absences of sharp peaks indicate that the structural disorder is dominant. The amorphous nature of the as-prepared sample has been confirmed through selected area electron diffraction (SAED) pattern shown in the inset of panel Fig. 1(a). The EPMA on as-prepared sample revealed the presence of Ni, B, (18−20 wt %) and oxygen that stem from the chemical reaction carried out under ambient conditions and in aqueous medium. As shown in Figs. 1(b) and 1(c) the FESEM and TEM images reveal the nanometer scale character of the particles with a narrow size distribution and a cottonlike morphology. The average diameter of the particle is estimated to be about ∼30 nm and can be influenced by the synthesis conditions. However, the present XRD, microscopy data show similar features that were reported by earlier workers.[22,23] The DSC scan on as-prepared samples show thermal effects at about 335−382 °C and 463 °C, which is in agreement with the results reported earlier on the Ni–B amorphous ribbons[22] and fine particles [see Fig. 1(d)].[20,23] In order to understand thermal stability and the evolution of crystalline phases, we have carried out structural investigation on samples annealed at 400 °C for 1 h, and also *in situ* XRD pattern taken at a temperature 350 °C under high vacuum conditions (10^{-6} mbar). Rietveld refinement analysis of the data has been performed on the XRD data and excellent fits were obtained which is evident from the residues shown in the Fig. 2. From this analysis it is also identified that the samples contain a two-phase mixture of the Ni$_3$B (80%) and Ni (20%) in the case of 350 °C annealed sample, while in the 400 °C annealed sample the volume fraction of Ni increases at the expense of Ni$_3$B (See Table I). These results are in agreement with the earlier reports[22] according to which the first exothermic peak observed at about

335 °C could be assigned to onset of crystallization process of amorphous matrix into nanocrystalline Ni and Ni$_3$B phase. A further rise in DSC curve on heating could be due to the increased fraction of Ni at the expense of disordered Ni$_3$B. Finally the crystallization process of Ni–B alloy is completed at 470 °C. From the XRD line broadening typical crystallite sizes of the Ni and Ni$_3$B were estimated using Scherrer formula, $D=k\lambda/(\beta_{eff} \cos \theta_{hkl})$, where k is the particle shape factor (generally taken as 0.9), λ is the wavelength of Cu $K\alpha$ radiation, θ_{hkl} is the Bragg angle of the peak corresponding to the (*hkl*) set of planes, and β_{eff} is defined as $\beta^2_{eff}=\beta^2_m -\beta^2_s$, where β_m and β_s are the full peak width at half the maximum (FWHM) intensity of the sample under investigation and the FWHM of a standard silicon sample, respectively. Comparison of the XRD line profiles with that of a standard silicon sample is done to eliminate the peak broadening due to instrumental beam divergence. It is interesting to point out here that the crystallite sizes obtained for Ni (Ni$_3$B) 350 and 400 °C annealed samples are 9 (19 nm) and 12 nm (25 nm), respectively. The Ni crystallite sizes are observed to be little larger than that reported in the literature on ribbon samples. These small variations are expected due to the small deviations in the composition and different preparation methods.[24]

Recent theoretical studies[14] suggest that by varying relative volume fraction of nickel and boron in Ni–B binary alloys and subsequently annealing the materials at suitable temperature in oxygen atmosphere, one can synthesize Ni:B$_2$O$_3$ composites. In order to study the evolution of Ni–B related phases, we have heat-treated the as-prepared sample at different temperatures in air and recorded the structural and magnetic data. The XRD patterns of (a) as-prepared powder and those annealed in air at (b) 300, (c) 400, and (d) 500 °C for 1 h are shown in Fig. 3. The sample annealed at 300 °C shows XRD peaks, which could be indexed as Ni$_3$B and fcc-Ni phases. A similar result has been observed on annealing at higher temperatures in high vacuum conditions [see Fig. 2(a)]. To our surprise, the 400 °C air annealed sample showed a single-phase fcc-Ni peaks, while all the Ni$_3$B peaks disappear in XRD pattern. The sample was further annealed at 500 °C in air with an expectation to obtain a NiO phase. However, contrary to our expectations sharp peaks in the XRD patterns were observed and identified as
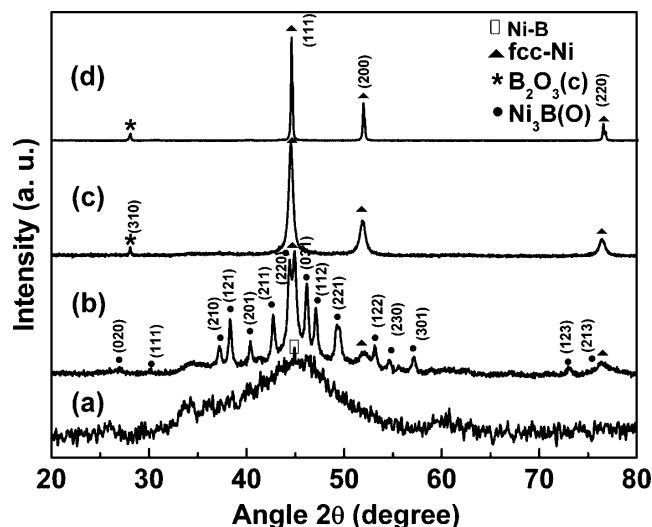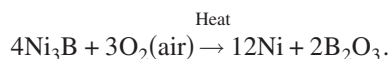
FIG. 3. X-ray diffractograms of (a) as-prepared and annealed at (b) 300, (c) 400, and (d) 500 °C in air atmosphere for 1 h.

FIG. 4. TEM micrographs of (a) 300 and (c) 500 °C air annealed samples and corresponding electron diffraction patterns in (b) and (d).

fcc-Ni. It is interesting to note that irrespective of annealing medium, we obtain fcc-Ni, when the samples were subjected to a heat treatment even at 500 °C. Further, on close observation of XRD patterns of air annealed samples, an additional unknown low intensity peak could be seen at 2θ =28°. The XRD peak broadening has significantly reduced when the sample was annealed at 500 °C as opposed to 400 °C. This observation suggests that the annealing at 500 °C only results in increase in crystallite size. From the XRD and DSC results it can be suggested that annealing in air at 300 °C results in Ni particles in metastable Ni_3B matrix. At higher temperatures (400 and 500 °C) the metastable Ni_3B further segregate into Ni at the same time boron reacts with oxygen and probably forms a B_2O_3 matrix. The absence of characteristic NiO XRD lines suggests that the Ni particles are embedded or encapsulated to the B_2O_3 matrix, which does not allow the oxidation of Ni.

$$(\text{amorphous})NiB \xrightarrow{\text{Heat}} Ni + Ni_3B,$$

$$4Ni_3B + 3O_2(\text{air}) \xrightarrow{\text{Heat}} 12Ni + 2B_2O_3.$$

Diminution of the Ni_3B phase on heat treatment in air could be due to the segregation of Ni from Ni_3B phase. Since we did not find elemental boron in XRD patterns, we presume that entire boron that was present in as-prepared samples is converted into B_2O_3 as shown in the above equation. The most intense XRD peak of crystalline B_2O_3 phase appears at 2θ=28°. Therefore, we assign the unknown peak observed in XRD pattern to B_2O_3 phase.[25] This suggests the possibility of existence of B_2O_3 crystalline phase in the sample along with dominant fcc-Ni. This conclusion is consistent with the x-ray photoelectron spectroscopy data[20] and the theoretical predictions.[14]

The microstructure was further investigated by TEM images and SAED patterns of annealed samples shown in Fig. 4. Figure 4(a) shows the TEM image of 300 °C air annealed sample, where one can see fine particles of Ni with average size 30 nm start growing along with Ni_3B. The correspond-

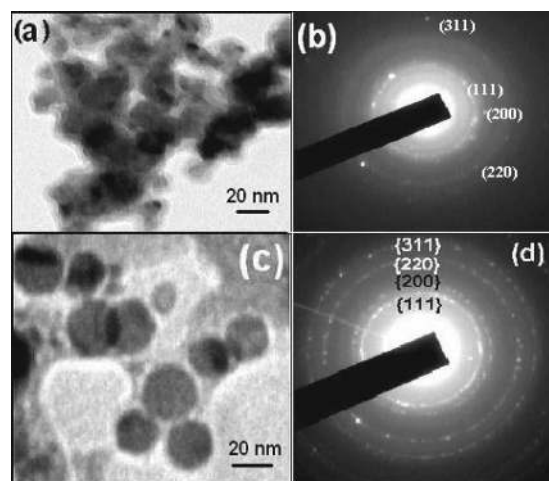ing SAED pattern [Fig. 4(b)] shows spots with diffused rings suggesting the presence of some structural disorder in the sample. However, TEM micrographs of 500 °C annealed sample [Fig. 4(c)] show well-developed Ni spherical particles with an average diameter of ~20 nm. On close observation of micrographs, the NPs appear to have core-shell geometry with inner Ni core and the outer B_2O_3 shell is clearly distinguished. The crystallite size of Ni is estimated from XRD peak broadening using Scherrer's formula is 30 nm, which is similar to the size observed in TEM micrographs. The ringlike SAED pattern [Fig. 4(d)] of the particles is typical of the pattern observed for the nanostructured fcc-Ni, which is consistent with the XRD results. The heat treatment in air results not only the development of spherical Ni NPs, but also significant changes in the morphology of the particles. These structural changes in the a-Ni–B to crystalline Ni involve in two-step process, which is evident from the XRD and TEM micrographs and supported by the two broad exothermic peaks observed in DSC. These observations are consistent with the earlier reports on rapidly solidified Ni–B ribbons and chemically prepared powders.

B. Magnetic properties

We split up our analysis of the magnetization results into two parts. (1) discusses the magnetic state of the as-prepared samples and explains the nonsaturating, hysteretic magnetization, (2) gives a plausible explanation for the enhanced magnetic properties on annealing in air.

1. Nonsaturating and hysteretic magnetization

The magnetization (M) as a function of applied field (H) has been recorded for as-prepared sample at 300 and 20 K. As shown in Fig. 5 the M-H curve at 300 K display low magnetization values along with an increase in magnetization at low magnetic fields but do not saturate at applied magnetic fields of 8 kOe (lower inset). On the other hand, 20 K magnetization data shows hysteresis curve (upper inset) with a significant increase in M value along with a strong nonsaturation behavior at higher applied fields. A large increase in coercivity (H_c) value of 200 Oe can also be seen in
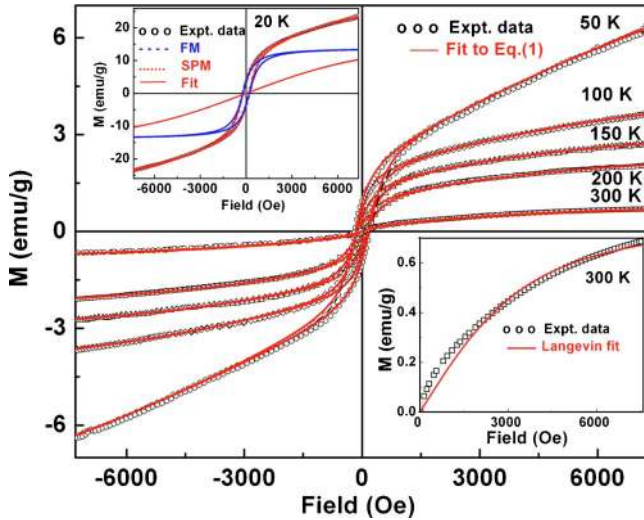
FIG. 5. (Color online) *M-H* plots of as-prepared sample at different temperatures along with the fits to the Eq. (1). The upper inset (upper) shows *M-H* curves of as-prepared sample ($T=20$ K) along with the fits (SPM +FM part) to Eq. (1) and the lower inset shows the initialization magnetization curve in conjunction with the fits to the Langevin function.

the *M-H* curve indicating a FM behavior at 20 K. In order to investigate whether the sharp rise in *M-H* curves at low field is due to interaction effects or FM component, hysteresis loops were recorded at various temperatures between 20 and 300 K. Several interesting features can be noted from this figure (main panel of Fig. 5): (i) At 300 K a nonhysteretic behavior is observed and the loop opens up as the temperature is lowered, (ii) a linear component in magnetization response with applied field is also observed to increase at low temperatures suggesting the existence of PM component along with FM behavior, and (iii) increased values of magnetization (M_s), remnant magnetization (M_r), and coercivity (H_c) on lowering the temperature. This behavior could be due to the presence of two magnetic components, i.e., a FM component that is easily saturated at low fields and a linear component could be considered SPM or PM. As shown in the figures the negligibly small area of measured loop and the slow approach to the saturation are a good indication of presence of a SPM phase. The presence of FM behavior is however, evidenced by the remnance magnetization and sharp increase in M at low fields. It is also important to note that the saturation of the magnetization could not be reached. These observations indicate that the FM component possibly stems from the strong intercluster interactions or distribution of cluster sizes with varying magnetic properties. As a first

approach for having an understanding of some of the above features, *M-H* curves of the as-prepared samples were fitted to the following expression[26] comprising a FM and a SPM part:

$$M(H) = \frac{2M_s}{\pi}\tan^{-1}\left[\frac{H \pm H_c}{H_c}\tan\left(\frac{\pi S}{2}\right)\right] + M_{SP}L\left[\frac{\mu_p H}{k_B T}\right].$$

(1)

The first term is the usual function customarily used to fit FM hysteresis curves while the second term accounts for the SPM component. The quantities M_s and H_c give, respectively, the saturation magnetization of the FM component and coercivity of the hysteresis loop. "S" is known as the "squareness" of the FM loop and is defined as the ratio of remnant magnetization to saturation magnetization of the FM component, i.e., $S = M_r/M_s$. The μ_p in the second term is the average magnetic moment per particle, $L(x) = \coth(x) - 1/x$ is the Langevin function (where $x = \mu_p H/k_B T$), and M_{SP} is the saturation magnetization. The solid lines through the data points shown in Fig. 5 are the fits to the Eq. (1). Reasonably good fits to the *M-H* have been obtained at various temperatures and the extracted fit parameters are presented in Table II. As shown in the table, "μ_p" value at 300 K is 1924 μ_B, which is in agreement with earlier observations on ribbon samples.[22,24] However, the particle moment is expected to be constant at low temperatures and to decrease when T approaches the Curie temperature (T_C), owing to the corresponding reduction in M_s. The parameter S for randomly oriented particles should be 0.5. In nanocomposites both exchange and dipolar interactions are present. The dipolar interactions tend to decrease the remnance, where as the exchange increases it. The increase in remnance at lower temperatures suggests the enhancement in exchange compared to the dipolar interactions. This is an indication that at low temperature the intercluster/intracluster interactions play a significant role.

2. Magnetic properties of air annealed samples

Magnetic hysteresis loops at 300 K for the as-prepared, 400 °C, and 500 °C air annealed (for 1 h) samples are shown in Fig. 6. The magnetic isotherms of as-prepared amorphous sample show a weak magnetic behavior while a FM component along with development of FM phase is clearly seen in air annealed samples. Further, magnetization values increase on annealing but no significant change in H_c is observed. As shown in Table III, the magnetic parameters,

TABLE II. Parameters extracted from SPM+PM fitting Eq. (1) for as-prepared sample at selected temperatures.

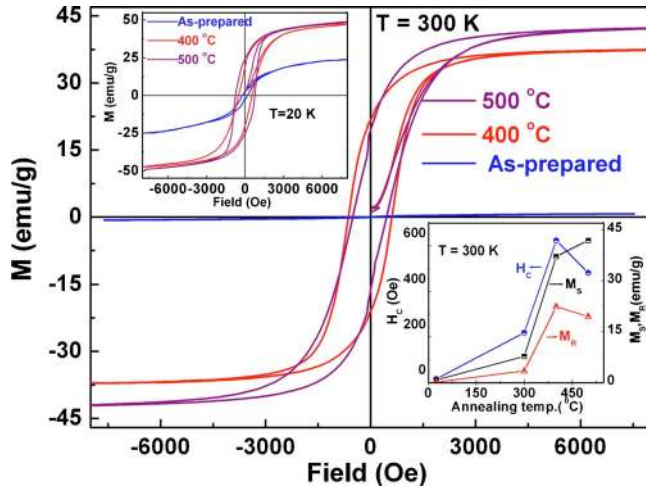| Temp. (K)	M_s (emu/g)	M_{sp} (emu/g)	H_c (Oe)	S	μ_p (μ_B)
300	0.1698	0.7577	33.75	0.0656	1924
200	1.245	1.4445	87.76	0.1507	969
150	1.6724	1.7842	108.56	0.2304	758
100	2.0887	3.0213	127.15	0.3151	398
50	2.4540	11.1377	189.99	0.3653	117
20	13.5398	18.7443	215.69	0.2719	85

FIG. 6. (Color online) Magnetic hysteresis curves measured at room temperature for as-prepared, air annealed at 400 and 500 °C samples. The upper inset gives M-H curve at 20 K and the lower inset shows the variation in coercivity, remnance, and saturation magnetization values at 300 K for the as-prepared and air annealed samples.

such as H_c and M_r values increase as the annealing temperature is increased up to 400 °C. However, when the samples were annealed at 500 °C, the M_r and H_c values decrease. As evident from the initial magnetization curves, the magnetization at lower fields shows a rapid increase with field, followed by saturation at a maximum field of 8 kOe. It can be seen that there is a significant change in magnetic parameters when the sample was subjected to heat treatment at 400 °C in air. This is in agreement with the structural data presented in Fig. 3(b), i.e., when the sample is annealed at 300 °C both Ni phase (20%) and Ni$_3$B phase (80%) grow simultaneously from a-NiB and the M_s value increases marginally as Ni$_3$B is PM (0.5 emu/g).[24] However, the disappearance of Ni$_3$B phase and development of strong nanocrystalline Ni phase in 400 °C annealed sample results in an abrupt increase in the M_s value. Further, annealing at 500 °C in air results in growth of crystallite size (see the reduced broadening in XRD peaks) of Ni and further enhances the M_s value. It is possible that the development of 20 nm spherical Ni particles (Fig. 4) at 500 °C results in reduction in shape anisotropy of the particle, which in turn reduces the H_c. It is interesting to point out that the observed M_s and H_c values of air annealed samples are considerably high compared to earlier reports.[7,27] This behavior is clearly associated with the growth of FM Ni spherical particle which are protected by the B$_2$O$_3$ nonmagnetic matrix. The higher H_c values could be

due to the single domain nature of the Ni. In order to verify this M-H measurements at $T = 20$ K have been performed for as-prepared, 400, and 500 °C air annealed samples and shown in the upper inset of Fig. 6. The as-prepared sample shows FM behavior at $T = 20$ K ($M_s \sim 25$ emu/g, $H_c \sim 200$ Oe) and the M_s values increase with annealing temperatures. This is consistent with the room temperature magnetization data and supports the argument that the increase in M_s is due to the reduction in PM component (Ni$_3$B). The M_s value is 47.5 emu/g at 20 K for 500 °C air annealed samples, which is about 82% of the bulk magnetization value of Ni. The low temperature M_s and H_c values of the present samples appear to be higher than that of Ni NPs,[27] carbon coated,[28] SiO$_2$,[7] and TiO$_2$ (Ref. 29) coated Ni particles reported in the literature. This enhancement in the magnetic parameters could be due the presence of single domain particles in the PM matrix.

Now we will turn our attention toward the temperature dependence of magnetic behavior. As the temperature is lowered from room temperature the ac susceptibility (χ_{ac}) goes through a broad maximum at around 80 K and on further lowering temperature a sharp peak appeared at 20 K in as-prepared sample [see Fig. 7(a)]. On the other hand, in 300 °C air annealed sample 20 K peak persists but the broad peak observed at about 80 K disappears probably due to formation of Ni-rich particles whose blocking temperature (T_B) > 300 K. The χ_{ac} monotonously decreases as the temperature is lowered for 500 °C annealed samples. These results along with structural and M-H data suggest that as-prepared sample has two types of magnetic entities one with weak magnetic moment and the other SPM clusters.[15,24] From the detailed magnetic investigations on similar samples, it was concluded that the residual magnetism is due to the contribution of small nickel particles, embedded in a PM amorphous matrix.[21,24] The Ni-rich region could be considered as clusters that behave like SPM as observed by Muniz et al.[24] while a-Ni–B matrix (PM at $T = 300$ K) can have a magnetically ordered state below 20 K. Zero field cooled (ZFC) and field cooled (FC) (in the presence of 100 Oe) magnetization curves for 300 °C annealed sample, shown in the Fig. 7(b), support this viewpoint. The samples annealed at 300 °C exhibits a hysteresis loop at 300 and 20 K (see inset of Fig. 7) but irreversibility in ZFC and FC curves is observed below 300 K followed by a steep increase in M for both FC and ZFC curves. This temperature corresponds to the low temperature peak in χ_{ac} that has been observed in both as-prepared and 300 °C annealed samples. On the other

TABLE III. Saturation magnetization (M_s), remnant magnetization (M_r), and coercivity (H_c) of the samples at 300 and 20 K.

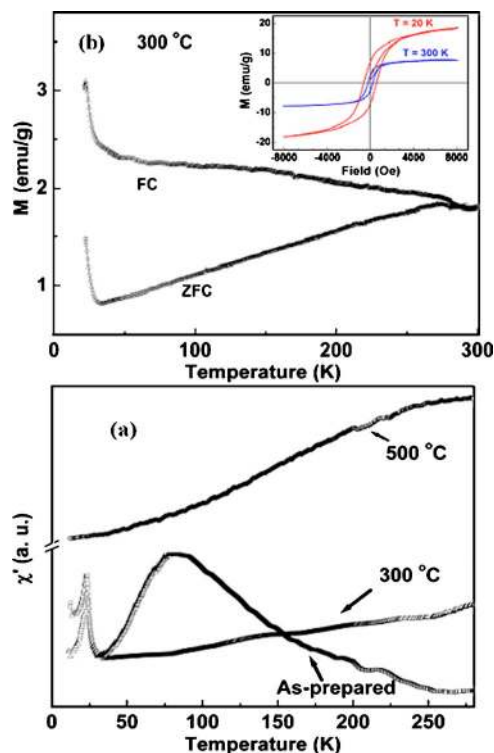|		$T = 300$ K			$T = 20$ K		
Sample	Phase	M_s (emu/g)	M_r (emu/g)	H_c (Oe)	M_s (emu/g)	M_r (emu/g)	H_c (Oe)
As-prep.	Ni–B	0.72	0.11	54	24.02	2.83	200
300 °C	Ni–Ni$_3$B	7.69	3.4	219	18.55	6.92	595
400 °C	Ni–B$_2$O$_3$	37.17	22.38	623	49.4	24.52	745
500 °C	Ni–B$_2$O$_3$	41.85	19.46	482	47.3	19.56	530

FIG. 7. (Color online) (a) ac susceptibility as a function of temperature for as-prepared, air annealed at 300 and 500 °C samples. (b) FC and ZFC magnetization as a function of temperature in 100 Oe applied field for air annealed 300 °C sample. Inset shows M-H curves at 300 and 20 K of air annealed 300 °C sample.

hand 400 and 500 °C annealed samples are FM as they exhibit well-defined hysteresis loops at $T=300$ K.

IV. DISCUSSION

From the structural analysis it is confirmed that the as-prepared powders are Ni-rich a-Ni–B. On annealing at 300 °C fcc-Ni and Ni_3B develop, which is clear from the XRD and magnetic measurements. Further, when heated in air above 400 °C, the crystalline Ni_3B converts into a B_2O_3 containing fcc-Ni spherical NPs with large increase in magnetization and coercivity values. In spite of annealing in air atmosphere no traces of NiO were found in XRD patterns. On the contrary, enhancement in M_s value has been observed, at the same time the increase in coercivity might be due to the decrease in intergranular exchange coupling and/or the increase in the number of pinning centers of B_2O_3 volume fraction increased on annealing in air. These results suggest that the FM nickel particles are encapsulated in B_2O_3 matrix, which protects the Ni core from the oxidation. Since there is no indication of the presence of NiO phases both in structural as well as magnetic data, we believe that Ni particle surface is not exposed to the air atmosphere, i.e., Ni is protected by B_2O_3 shell/matrix.[30] It is now well accepted that the Ni-rich a-NiB crystallizes into $Ni+Ni_3B$ phase. Here we extended this proposition through our structural and magnetic data analysis that annealing in air results in formation of Ni and B_2O_3 core-shell structure. A pertinent question now is that why oxygen reacts with B to form B_2O_3 shell first, rather than reacting with Ni to form NiO? For the ele-
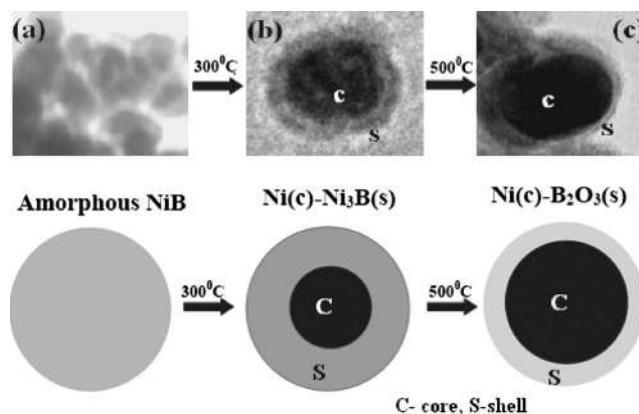

FIG. 8. Schematic phenomenological model along with TEM images indicating the evolution of core-shell structure during heat treatment in air.

ments of B, Ni, and H, since the bond energy of B–O bond (806 kJ/mol) is about two times larger than that of Ni–O bond (382 kJ/mol) and H–O (427 kJ/mol) at 298 K,[13,31] the oxygen would preferentially combine with boron to form suitable B_2O_3. This also suggests that the boron present on the surface of the particle would react with oxygen at this temperature and forms as a shell on Ni core. On the other hand an argument can also be presented on the basis of energy considerations, i.e., Gibbs free energy for NiO is −211 kJ/mol while for B_2O_3 it is −1194 kJ/mol,[31] which is much smaller than that of NiO, suggesting the lower energy values favor the formation of B_2O_3 shell. A phenomenological model for the evolution of $Ni:B_2O_3$ core-shell structure from a-Ni–B particles is presented in Fig. 8, along with the high resolution TEM images of the particle. A particle of the as-prepared sample, which is in amorphous state [Fig. 8(a)] when subjected to annealing in air at 300 °C, first thermal treatment results in formation of two phase mixture, i.e., Ni and Ni_3B phases as can be seen from contrast differences in the TEM image [Fig. 8(b)]. The outer layer could be the Ni_3B phase. On annealing at 500 °C the particle further develops into a nickel coated with thin layer of B_2O_3 [Fig. 8(c)], providing large values of magnetization. It is possible that annealing at higher temperatures, the B_2O_3 may react with Ni and can result in formation of nickel borate. However, low temperature thermal treatment presents FM particles protected by B_2O_3 matrix, can be useful for several room temperature applications.

V. SUMMARY AND CONCLUSIONS

In summary, a novel method of synthesis of core-shell structured magnetic $Ni:B_2O_3$ NPs has been proposed. The synthesis follows a two-step process: in the first step a-Ni–B powders were prepared by conventional borohydride reduction method and in the second stage devitrification of Ni–B powders in the air atmosphere at various temperatures results in formation of $Ni:B_2O_3$ core-shell structure. Structural and thermal analysis data on this sample shows that the evolution of Ni_3B and Ni phase and on further annealing a higher temperatures growth of $Ni:B_2O_3$ core-shell structure NPs. The presence of B_2O_3 outer layer inhibits the growth of nickel clusters and preserved the spherical shape during the

controlled annealing process, which has a very favorable effect on the coercivity and the squareness of the metal samples. Although the as-prepared sample exhibits weak magnetic properties due to the amorphous nature, the magnetic properties of the sample have improved significantly by a subsequent annealing at $300-500$ °C in air. The annealed sample display strong FM behavior with high $H_c \sim 623$ Oe and $M_s(\sim 42$ emu/g) values at 300 K compared earlier reports on Ni NPs. This suggests these NPs may have significant potential as recording media.

ACKNOWLEDGMENTS

[1] C. C. Berry and S. G. Curtis, J. Phys. D **36**, R198 (2003).

[2] V. Skumryev, S. Stoyanov, Y. Zhang, G. Hadjipanayis, D. Givord, and J. Nogues, Nature (London) **423**, 850 (2003).

[3] Q. A. Pankhurst, J. Connolly, S. K. Jones, and J. Dobson, J. Phys. D **36**, R167 (2003).

[4] T. Hayashi, S. Hirono, M. Tomita, and S. Umemura, Nature (London) **381**, 772 (1996).

[5] F. Bodker, S. Morup, S. W. Charles, and S. Linderoth, J. Magn. Magn. Mater. **196–197**, 18 (1999).

[6] L. Savini, E. Bonetti, L. D. Bianco, L. Pasquini, L. Signorini, M. Coisson, and V. Selvaggini, J. Magn. Magn. Mater. **262**, 56 (2003).

[7] F. C. Fonseca, G. F. Goya, R. F. Jardin, R. Muecillo, N. L. V. Carreno, E. Longo, and E. R. Leite, Phys. Rev. B **66**, 104406 (2002).

[8] W. Liu, W. Zhonga, H. Y. Jiang, N. J. Tang, X. L. Wu, and W. Y. Du, Eur. Phys. J. B **46**, 471 (2005).

[9] J. Jiao, S. Seraphin, X. Wang, and J. C. Withers, J. Appl. Phys. **80**, 103 (1996).

[10] H. Tokoro, S. Fujii, and T. Oku, J. Mater. Chem. **14**, 253 (2004).

[11] C. P. Luo, S. H. Liou, L. Gao, Y. Liu, and D. J. Sellmyer, Appl. Phys. Lett. **77**, 2225 (2000).

[12] Z. D. Zhang, J. L. Yu, J. G. Zheng, I. Skorvanek, J. Kovac, X. L. Dong, Z. J. Li, S. R. Jin, H. C. Yang, Z. J. Guo, W. Liu, and X. G. Zhao, Phys. Rev. B **64**, 024404 (2001).

[13] X. F. Zhang, X. L. Dong, H. Huang, B. Lv, J. P. Lei, S. Ma, W. Liu, and Z. D. Zhang, Mater. Sci. Eng., B **143**, 76 (2007).

[14] H. Yamamoto and M. Morishita, J. Alloys Compd. **438**, L1 (2007) (and references therein).

[15] J. M. Rojo, A. Hernando, M. El Ghannami, A. Garcia-Escorial, and M. A. Gonzalez, Phys. Rev. Lett. **76**, 4833 (1996).

[16] Z. L. Schaefer, X. Ke, P. Schiffer, and R. E. Schaak, J. Phys. Chem. C **112**, 19846 (2008).

[17] J. V. Wonterghem, S. Mørup, C. J. W. Koch, S. W. Charles, and S. Wells, Nature (London) **322**, 622 (1986).

[18] S. Linderoth and S. Morup, J. Appl. Phys. **69**, 5256 (1991).

[19] J. Geng, D. A. Jefferson, and B. F. G. Johnson, Chem. Commun. (Cambridge) **2007**, 969.

[20] H. Li, H. Li, and J.-F. Deng, Mater. Lett. **50**, 41 (2001).

[21] I. Bakonyi, E. Babic, M. Miljak, R. Luck, J. Bahle, R. Hasegawa, and J. Kollar, Phys. Rev. B **65**, 104423 (2002).

[22] P. Muniz, J. A. De Toro, and J. M. Riveiro, J. Magn. Magn. Mater. **272–276**, e1129 (2004); J. M. Riveiro, P. Muniz, J. P. Andres, and J. A. De Toro, ibid. **188**, 153 (1998).

[23] S. Wei, H. Oyanagi, Z. Li, X. Zhang, W. Liu, S. Yin, and X. Wang, Phys. Rev. B **63**, 224201 (2001).

[24] P. Muniz, J. A. De Toro, and J. M. Riveiro, Phys. Rev. B **66**, 104101 (2002).

[25] V. G. de Resende, G. M. da Costa, E. De Grave, and L. Datas, J. Mater. Sci. **41**, 6843 (2006); A. Oki, L. Adams, and Z. Luo, Inorg. Chem. Commun. **11**, 275 (2008).

[26] M. B. Stearns and Y. Cheng, J. Appl. Phys. **75**, 6894 (1994).

[27] S. Vitta, J. Appl. Phys. **101**, 063901 (2007); Y. W. Du, M. X. Xu, J. Wu, Y. B. Shi, and H. X. Lu, ibid. **70**, 5903 (1991).

[28] V. Singh, S. Ram, M. Ranot, J. G. Park, and V. Srinivas, Appl. Phys. Lett. **92**, 253104 (2008).

[29] S. Zhu, L. M. Wang, X. T. Zu, and X. Xiang, Appl. Phys. Lett. **88**, 943107 (2006).

[30] In Fourier transform infrared spectra, three intense peaks at 1446, 1194, and 796 cm^{-1} were observed which arise due to B–O stretching and vibration planes in air annealed samples, which is an indication of the presence of B_2O_3 phase on the surface of the particles.

[31] D. R. Lide, in *CRC Handbook of Chemistry and Physics*, 81st ed., edited by D. R. Lide (CRC, Boca Raton, 2000).